IOP PUBLISHING JOURNAL OF PHYSICS: CONDENSED MATTER

J. Phys.: Condens. Matter **19** (2007) 446210 (13pp) doi:10.1088/0953-8984/19/44/446210

Structure and magnetic properties of the weak ferromagnet $Sr_{2-x}La_xIrO_4$

Carlos Cosio-Castaneda[1], Gustavo Tavizon[1], Alejandro Baeza[2], Pablo de la Mora[3] and Roberto Escudero[4]

[1] Departamento de Física y Química Teórica, Facultad de Química, Universidad Nacional Autónoma de México, Ciudad Universitaria 04510, México, DF, Mexico
[2] Departamento de Química Analítica, Facultad de Química, Universidad Nacional Autónoma de México, Ciudad Universitaria 04510, México, DF, Mexico
[3] Departamento de Física, Facultad de Ciencias, Universidad Nacional Autónoma de México, Ciudad Universitaria 04510, México, DF, Mexico
[4] Instituto de Investigaciones en Materiales, Universidad Nacional Autónoma de México, Ciudad Universitaria 04510, México, DF, Mexico

E-mail: gtavizon@servidor.unam.mx

Received 29 May 2007, in final form 31 August 2007
Published 18 October 2007
Online at stacks.iop.org/JPhysCM/19/446210

Abstract

The 5d electron-based $Sr_{2-x}La_xIrO_4$ system ($0 \leqslant x \leqslant 0.2$) has been synthesized by a solid-state route. The $x = 0$ composition is a nonmetallic weak ferromagnet with a Curie temperature at about 240 K. The crystal structure behaviour and magnetic properties exhibited by this $Sr_{2-x}La_xIrO_4$ system can be explained on the basis of the extended character of the 5d electrons of the Ir cation and its valence states. Rietveld analysis of x-ray powder diffraction on Sr_2IrO_4 agrees well with previous structural neutron experiments. Furthermore, density functional theory (DFT) calculations predict that $I4_1/acd$ represents a more stable crystal structure than K_2NiF_4 ($I4/mmm$). Electrical resistivity and magnetic properties of $Sr_{2-x}La_xIrO_4$ are strongly dependent on the Ir^{3+} content. The $Sr_{2-x}La_xIrO_4$ magnetic behaviour in the range of 2–240 K can be ascribed to a weak ferromagnet, produced by an array of canted antiferromagnetically ordered Ir^{4+} magnetic moments.

(Some figures in this article are in colour only in the electronic version)

1. Introduction

Transition metal oxides (TMO) with the layered K_2NiF_4-type structure have long been studied, mainly because they display a wide variety of unusual structural and magnetic properties [1, 2]. From the chemical point of view, the TMO with K_2NiF_4 structure show a wide variety of heterogeneous catalytic activity associated with their capability to induce oxidative reactions [3]. Most of the investigations on TMO have been focused on systems

containing 3d electron orbitals, and within these kinds of compounds, the copper-oxide based superconductors have attracted much interest over the past twenty years. On the other hand, the detailed electronic properties of 4d-and 5d-based compounds have been largely unexplored. There are several characteristics that could be associated with the extended character of 4d and 5d electron orbitals, in contrast to those observed in 3d metal-oxides (MO). In these kinds of systems the large spatial extent of the 4d and 5d electron metal-orbitals that participate in the metal–oxygen bonding enable an enhanced d–p hybridization that affects this bonding. As a consequence, the structural and magnetic properties of those systems are expected to be different from that observed in 3d metal-oxide systems. In the $A_{n+1}Ir_nO_{3n+1}$ (A = Sr, Ba) Ruddlesden–Popper series of layered iridiates, the case of $n = \infty$, $BaIrO_3$ has attracted a great deal of attention due to the unexpected electrical and magnetic properties [4–7]. Also related to 5d systems is the superconductivity found in the Os- and Re-based pyrochlore oxides [8]; accordingly, more attention should be paid to the 5d TMO. For this third-row, 5d electron systems, there is only one MO, Sr_2IrO_4, which is expected to have the K_2NiF_4-type structure. From the structural point of view, this system possesses a highly symmetric crystal structure that permits the study of the physical and chemical properties in a more direct way.

Sr_2IrO_4 was at first assigned to the $I4/mmm$ space group (SG) [9]. However, electron diffraction studies on the $Sr_2Ru_{1-x}Ir_xO_4$ system [10] suggested a different crystal structure for Sr_2IrO_4, the less symmetric $I4_1/acd$ SG [1]. This SG assignment was subsequently corroborated by neutron diffraction experiments [11]. In spite of the expected similarities between Sr_2RuO_4 and Sr_2IrO_4, the former does crystallize in the $I4/mmm$ SG.

For Sr_2IrO_4 in the $I4/mmm$ symmetry, the Ir atom would be in an octahedron that is aligned along the crystal axes; in the $I4_1/acd$ symmetry this octahedron is rotated by $\sim 11^\circ$ around the c-axis. This rotation alternates to the right and to the left along the a- and b-axes. The oxygen atom between two Ir atoms along the a-axis (Ir–O–Ir) is displaced in the b-direction due to this rotation. In the upper layer, the oxygen atom is displaced in the a-direction, and in the next in the $-b$-direction, and so on, forming a spiral. The modified cell is four times larger: $\sqrt{2} \times \sqrt{2} \times 2$ [1, 11].

As expected from the crystal field configuration of most of the 5d compounds, the Ir^{4+} ions are assumed to be in the $[Xe]4f^{14}5d^5$ electronic configuration and in the low spin $t_{2g}^5e_g^0$ state [12–14], with the ground state being $^2T_{2g}$. On the other hand, neutron diffraction experimental results indicate that the apical Ir–O distance is greater than the equatorial Ir–O distance (2.067 and 1.983 Å, respectively [11]). These distances suggest the existence of degeneracy in the d_{xz} and d_{yz} orbitals and the unpaired electron occupying the half-filled d_{xy} orbital [15]. Thus the ground state for Ir^{4+} in Sr_2IrO_4 is expected to have a multiplicity $M = 2$ ($S = 1/2$). The difference between the apical and equatorial distances has been previously associated to a Jahn–Teller distortion [1].

When considering magnetic properties of Sr_2IrO_4, due to the extended character of the 5d orbitals, the electron repulsion effects are small and the exchange terms favouring parallel spin configurations are negligible. On the other hand, the normal superexchange bonding contribution is more important than the corresponding ferromagnetic exchange and an antiferromagnetic arrangement of Ir^{4+}–O–Ir^{4+} spins would be expected. Due to the rotation of the IrO_6 octahedra, the centre of inversion located on the oxygen of the Ir^{4+}–O–Ir^{4+} group is removed; with this, due to the Moriya rules [1, 16, 17], a non-collinear antiferromagnetic ordering is now allowed and the antiferromagnetically ordered spins no longer cancel. This non-collinear spin arrangement is the result of a type of magnetic interaction known as Dzyaloshinskii–Moriya (DM) [17, 18].

In this work, we report a study of the structural and magnetic properties of the solid solution $Sr_{2-x}La_xIrO_4$. By means of the lanthanum substitution on sites of Sr, we intend to

change the oxidation state of iridium from Ir^{4+} to Ir^{3+} in order to obtain a low spin state with the $t_{2g}^6 e_g^0$ configuration. With this change, the magnetic interaction between contiguous Ir moments is expected to diminish. The Ir^{3+} content in samples has been confirmed by cyclic voltammetry with modified carbon paste electrodes (MCPE), since these kinds of electrodes have been successfully used to analyse low soluble redox compounds [19, 20]. On the side of electrical properties, a change in the oxidation state of Ir is expected to lead to more resistive samples, because two electrons will be occupying the d_{xy} orbital. In the case of the isovalent substitution of Sr by Ca or Ba, there are no remarkable effects on the magnetic and electrical properties of Sr_2IrO_4, in spite of structural changes [21]. In order to understand the preference for a less symmetric crystal structure of Sr_2IrO_4 (from $I4/mmm$ to $I4_1/acd$), we also have performed an *ab initio* optimization of geometry, and these results are compared against those obtained via Rietveld refinement. The main purpose of this work is to provide additional experimental facts to discern whether the small magnetic moment of Ir in Sr_2IrO_4 comes from the spin polarization (resulting from the difference in the occupation of the up and down spin states of the t_{2g}-block bands (itinerant magnetism)), or whether the system can be described on the basis of localized states, and the magnetic behaviour of Sr_2IrO_4 as that corresponding to a canted antiferromagnet that results via the Dzyaloshinskii–Moriya anisotropic superexchange interaction.

2. Experimental details and computational procedure

Polycrystalline samples of $Sr_{2-x}La_xIrO_4$ ($x = 0$, 0.05, 0.1, 0.15, 0.20) used in this study were synthesized through the conventional solid-state reaction method. The starting materials were iridium (99.9%), strontium carbonate (99.995%), and lanthanum oxide (99.99%). These chemicals were mixed and polycrystalline samples of the solid solution $Sr_{2-x}La_xIrO_4$ were obtained by heating for 15 min at 1423 K in air, regrinding the sample and heating again for 15 min. Finally, the samples were pressed into pellets and heated at 1323 K for 120 min followed by quenching in air. The reactions were carried out in high-alumina combustion boats. The formation of single-phase compositions in the range $0.0 \leqslant x \leqslant 0.20$ was confirmed by powder x-ray diffraction analysis using a Siemens D-5000 x-ray diffractometer in Debye–Scherrer geometry.

The MCPE was constructed by mixing 25 mg of spectroscopic graphite (Aldrich, particle size <0.45 mm), 10 mg of Nujol and 10 mg of the iridium sample. This mixture was placed in a small polyethylene tube with 0.017 cm^2 of surface area, the connection was made with carbon rods. Cyclic electrochemical measurements were done in a 2 ml cell with 1.0 ml of 0.1 M KNO_3 as supporting electrode connected to a potentiostat (BAS CV-27). The measurements were done with an Ag/AgCl reference microelectrode and a glassy carbon disc (0.07 cm^2). The initial potential was -0.95 V, the inversion potential 1.2 V, and the scan rate 0.1 V s^{-1}.

Temperature dependence of electrical resistivity of the samples was measured in a bar geometry, using the four-contact technique with Ag paint electrodes in the range of 15–300 K. Magnetic behaviour of samples was determined on polycrystalline pellets in a SQUID magnetometer (Quantum Design MPMS), first, at different fields (0.1–2.0 T) for all the samples (magnetic susceptibility versus temperature), then, changing temperature at several fields for compounds with $x = 0$ and 0.15 (magnetization versus field isotherms).

In order to distinguish between the two alternative space groups $I4/mmm$ and $I4_1/acd$, full potential all electron quantum mechanical calculations were done with the WIEN2k package [22], which is a linearized augmented plane wave (FP-LAPW) method based on DFT.

The generalized gradient approximation of Perdew *et al* [23] was used for the treatment of the exchange–correlation interactions. The energy threshold to separate localized and non-localized electronic states was −6 Ryd. The muffin-tin radii were: 2.0 a_0 for strontium, 2.1 a_0 for iridium, and 1.56 a_0 for oxygen (a_0 is the Bohr radius).

3. Results and discussion

3.1. Structure characterization

X-ray powder diffraction showed that the solid solution $Sr_{2-x}La_xIrO_4$ exists in the $0.0 \leqslant x \leqslant 0.20$ range. For compositions with $x > 0.20$ an additional phase is formed; this extra-phase was identified as not belonging to the Ruddlesden–Popper series, $Sr_{n+1}Ir_nO_{3_{n+1}}$. Detailed Rietveld analysis [24] of x-ray diffraction data gives as a result two possible space groups; $I4/mmm$ and $I4_1/acd$.

Quantum mechanical calculations were done on the $x = 0$ sample (Sr_2IrO_4) in order to discriminate between these two alternatives. To obtain reliable results these calculations were made with high accuracy; for the number of plane waves the criterion that was used is that $R_{\mathrm{MT}}^{\mathrm{min}}$ (muffin tin radius) $\times$ K_{max} (for the plane waves) $= 9$, for the number of k-points, the number was $17 \times 17 \times 17$ for the $I4/mmm$ symmetry, and $11 \times 11 \times 11$ for $I4_1/acd$. These calculations give (a) total energies, which would show which symmetry is more stable; and (b) forces on the atoms, which can be used to obtain the optimized geometry.

The main difference between these two symmetries is that the IrO_6 octahedra in the $I4_1/acd$ SG are rotated by $\sim 11^\circ$ around the z axis, in other words, the in-plane oxygen position in the $I4/mmm$ symmetry is in (1/2, 0, 0), and with the rotation of the octahedron this oxygen is displaced in the y direction, $(1/2, y, 0)$ (the other oxygen atoms in the octahedron are displaced in their respective directions, also the rotation of the octahedra alternates along the a and b directions, and the unit cell in the $I4_1/acd$ symmetry is larger).

The energy results show an important difference, the $I4_1/acd$ symmetry is more stable by 0.59 eV/f.u., which suggests that this symmetry is the correct one. When calculating the forces, the chosen starting point was the $I4_1/acd$ symmetry with the in-plane oxygen in $(1/2, y, 0)$ with a very small y. If, as a result, a force is found pointing towards a smaller y, that is, towards (1/2, 0, 0), then the symmetry would reduce to the $I4/mmm$ SG. The force found was in the opposite direction. After this, the internal coordinate of this oxygen atom was then optimized and full relaxation gave a rotation of the IrO_6 octahedron of 9.686°; this angle being quite close to the one obtained by our Rietveld refinements, 9.32°, and by neutron diffraction experiments, 11° [11]. With this result we consider that Sr_2IrO_4 belongs to the $I4_1/acd$ SG. Partial substitution of Sr, which is outside the IrO_6 octahedron, by La, should not affect the SG symmetry. X-ray powder diffraction data of $Sr_{2-x}La_xIrO_4$ produced the following values for the rotation of the IrO_6 octahedra, about the c-axes: 9.32°, 10.2°, 7.07°, 7.07°, and 5.93° for $x = 0$, 0.05, 0.10, 0.15, and 0.20, respectively.

Table 1 shows the crystal cell and octahedron parameters for several compositions of $Sr_{2-x}La_xIrO_4$ at room temperature, determined by Rietveld analyses of the x-ray diffraction data [24]. The reduction of the c-cell parameter and the elongation of the *in-plane*-cell parameters, see figure 1, can be explained in the following way. The IrO_6 octahedron is initially elongated due to the Jahn–Teller effect. This distortion is reduced with the Ir^{3+}:$(t_{2g})^6$ introduction in the crystal cell due to the $Sr^{2+} \rightarrow La^{3+}$ ion substitution (table 1); the extra charge contributed by La^{3+} fills the Ir:d_{xy} producing a larger Ir^{3+}, the Jahn–Teller distortion is reduced and the octahedron becomes more symmetric, that is, the apical Ir–O bond decreases. Also the in-plane Ir–O bonds should increase (Ir^{3+} (0.68 Å) is bigger than Ir^{4+} (0.63 Å) [25]),

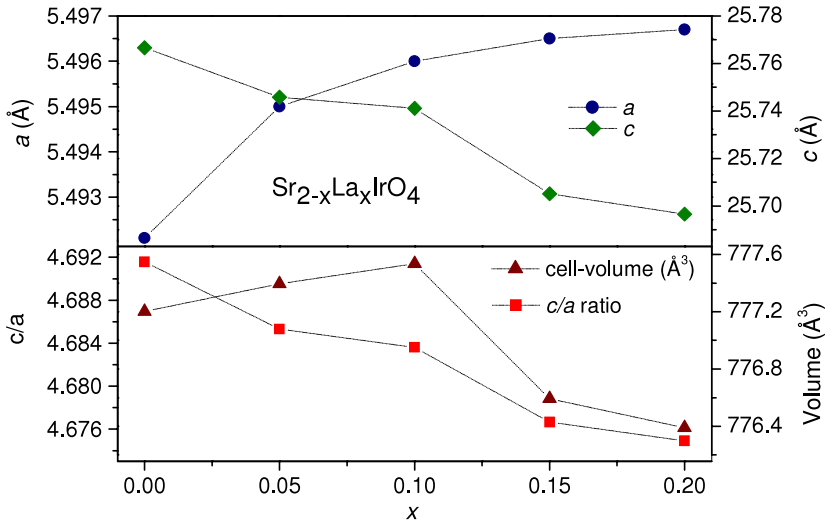

Figure 1. Cell-parameters, volume, and c/a ratio of $Sr_{2-x}La_xIrO_4$ as a function of x. Unit cell parameters were determined from structural Rietveld refinements.

Table 1. Unit cell parameters, equatorial (A), and apical (C) Ir–O bond lengths in the IrO_6 octahedron of $Sr_{2-x}La_xIrO_4$. φ represents the bond angle formed by O–Ir–O of two contiguous octahedra. A, C, and φ were calculated from the results of Rietveld refinements.

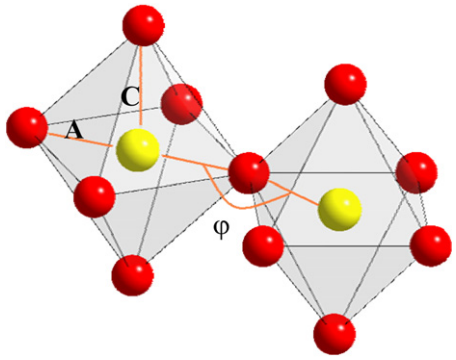

	Sr_2IrO_4	$Sr_{1.95}La_{0.05}IrO_4$	$Sr_{1.9}La_{0.1}IrO_4$	$Sr_{1.85}La_{0.15}IrO_4$	$Sr_{1.8}La_{0.2}IrO_4$
a-cell parameter (Å)	5.4921 (8)	5.4950 (1)	5.4960 (1)	5.4965 (1)	5.4967 (1)
c-cell parameter (Å)	25.7666 (6)	25.7458 (8)	25.7411 (8)	25.7052 (1)	25.6966 (1)
A (Å)	1.968	1.947	1.958	1.958	1.954
C (Å)	2.301	2.075	1.969	1.897	1.922
φ (deg)	161.37	159.59	165.86	165.86	168.13

although this is not the observed tendency. The rotation of the octahedra is reduced with x, this is probably due to the filling of the Ir:d_{xy} and the in-plane O:p_σ that forces the Ir–O–Ir bond angle towards 180°. The c-parameter reduction is a consequence of this octahedron modification, but also the $Sr^{2+} \rightarrow La^{3+}$ ion substitution reduces this parameter further ($r^{2+}_{Sr} = 1.21$ Å, $r^{3+}_{La} = 1.1$ Å, both for CN $= 7$ [25]). The in-plane parameters increase because of the rotation of the octahedra.

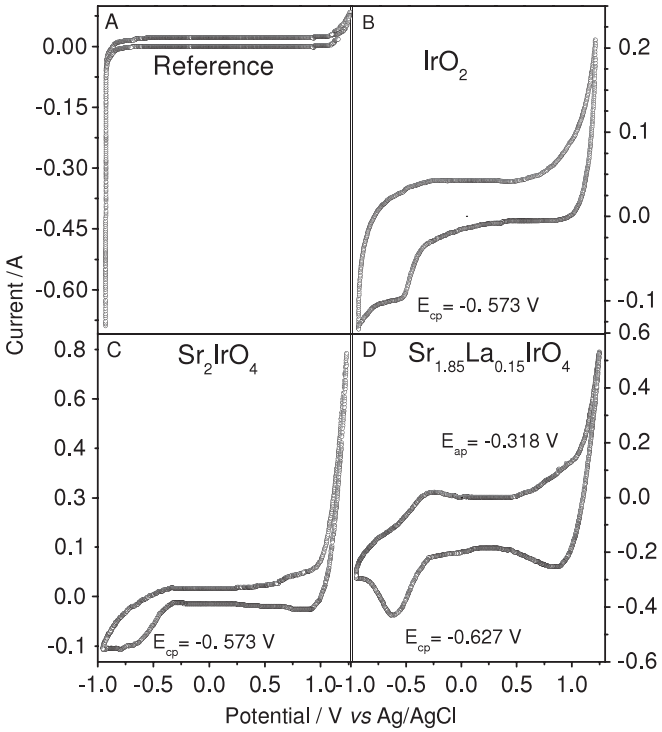

Figure 2. Four cyclic voltammograms obtained with the MCPE. (A) The reference system, carbon–Nujol paste (no iridium sample added), which shows a clean background current with no electrochemical signals due to CPE or supporting electrolyte; (B) IrO_2 obtained from high-purity metallic iridium; (C) Sr_2IrO_4 sample; and (D) $Sr_{1.85}La_{0.15}IrO_4$ sample. In (B)–(D) the potential values for the anodic (E_{ap}) and cathodic peaks (E_{cp}) are also shown.

3.2. Electrochemical detection of Ir^{3+}

As shown in figures 2(B) and (C), no oxidation peak is observed, but a well-defined reduction peak at $E_{cp} = -0.573$ V due to Ir^{4+} is found in both samples. These peaks correspond to a reversible monoelectronic reduction when compared with a ferrocene/ferrocinium (Fe^{3+}/Fe^{2+}) MCPE standard in the same voltammetry conditions (not shown). In figure 2(D) an anodic peak at $E_{ap} = -0.318$ V and a cathodic peak at $E_{cp} = -0.627$ V are observed. The position of the anodic peak permits the assignation of this signal to the $Ir^{3+} \rightarrow Ir^{4+}$ oxidation process, due to the presence of Ir^{3+} in the original sample, $Sr_{1.85}La_{0.15}IrO_4$ [20, 26].

3.3. Resistivity measurements

The temperature dependence of resistivity for polycrystalline samples of the $Sr_{2-x}La_xIrO_4$ solid solution are shown in figure 3. All samples exhibit semiconducting temperature dependence below 300 K. However, these curves do not correspond to an activated process for the whole temperature range. For temperatures above 200 K, the resistivity data could be approximated by the thermal activation law, $\rho \sim \exp(-E_a/k_BT)$, where E_a and k_B stand for the activation energy and the Boltzmann constant, respectively. The fitting for the thermally activated process at $T > 200$ K is shown in the inset of figure 3, and it is possible to observe that the value for the activation energy increases with the lanthanum content of samples. The activation energy

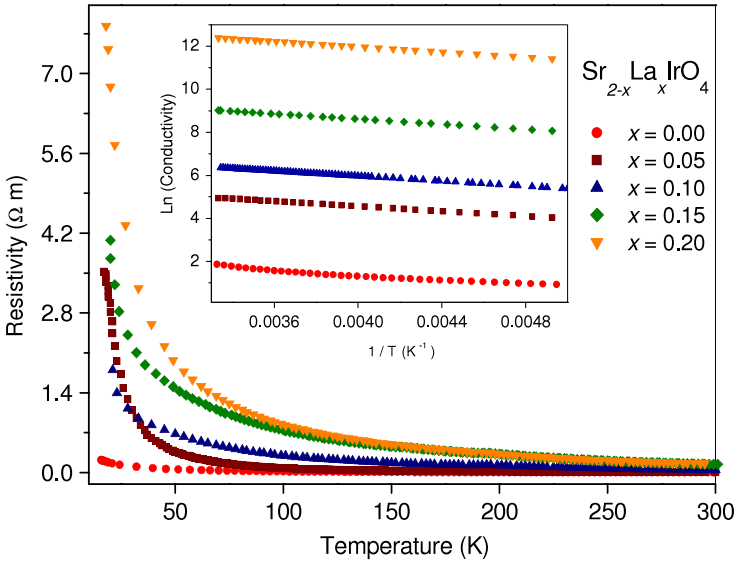

Figure 3. Temperature dependence of the electrical resistivity in the solid solution: $Sr_{2-x}La_xIrO_4$ ($0 \leqslant x \leqslant 0.20$). Inset shows a detail of the Arrhenius fitting for the 220 K $\leqslant T \leqslant$ 300 K range to obtain the activation energy values.

values for $Sr_{2-x}La_xIrO_4$ are 0.047, 0.049, 0.051, 0.052, and 0.055 eV for $x = 0$, 0.05, 0.10, 0.15, and 0.20, respectively [27]. These values are of the same order as those reported for the isovalent substitution of Sr by Ca and Ba in the solid solution $Sr_{2-x}A_xIrO_4$ (A = Ca and Ba) [21], but in the case of $Sr_{2-x}La_xIrO_4$ E_a increases with the La content of samples. The value for $x = 0$ is of the same order as the value recently reported by Kini *et al* [29]. It is worth mentioning that we did not find any indication of a transition to a metallic conduction, as was observed in both *a*- and *c*-directions by Cao *et al* [30] around 50–100 K in single crystal Sr_2IrO_4.

All samples of the solid solution $Sr_{2-x}La_xIrO_4$ exhibit semiconducting temperature dependence below 300 K. The gap-type temperature dependence of resistivity ($\rho \sim \exp(-E_a/k_BT)$), can be associated with the presence of a trivalent state of iridium. Assuming the same oxygen content in $Sr_{2-x}La_xIrO_4$ samples [28], when strontium is substituted by lanthanum, the electroneutrality condition forces iridium to change its valence state. Such change would imply a change in its electronic low spin configuration, from $(t_{2g})^5$, for Ir^{4+}, to $(t_{2g})^6$, for Ir^{3+}; in this way the d_{xy} orbital is no longer half-occupied, and one of the e_g orbitals, higher in energy, would get involved in the conduction process. When electrical resistivity data of $Sr_{2-x}La_xIrO_4$ samples does not behave according to the Arrhenius thermal activation law, as occurs in the low temperature range, it is possible to fit the data to the variable range hopping (VRH) equation. The temperature dependence of resistivity below 160 K obeys a law of the form $\rho \sim \exp(T_O/T)^\nu$ with $\nu = 1/4$, this value is thought to be associated with the three-dimensional variable range hopping of carriers between states localized by disorder, implicating negligible long-range Coulomb repulsions between electrons in this range of temperature. Similar localized behaviour has been also deduced from the *ab* plane measurements of resistivity in $Sr_3Ir_2O_7$ [6].

Electrical properties of $Sr_{2-x}La_xIrO_4$ can be understood beginning from the insulator behaviour of Sr_2IrO_4. As suggested by Huang *et al* [11], two elements account for this insulator

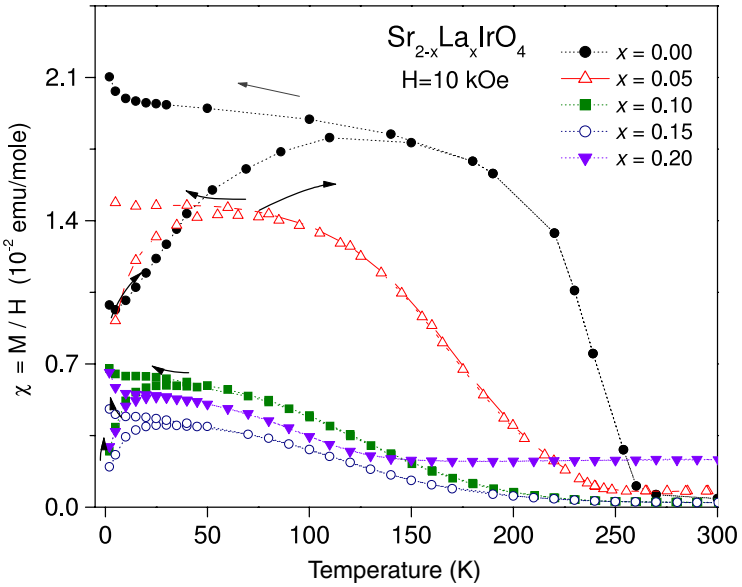

Figure 4. Temperature dependence of the magnetic susceptibility of $Sr_{2-x}La_xIrO_4$, $H = 10$ kOe. The arrows to the right correspond to ZFC (the sample was cooled in zero field and then heated), while the arrows to the left correspond to FC. Note how the irreversibility temperature (IT) diminishes with La content.

character. On one side, the elongation of the Ir–O bond along the *c*-axis (*C* parameter in the figure of table 1) is indicative of how the t_{2g} orbitals are split: there is a degenerate state that contains the d_{xz} and d_{yz} orbitals, and at higher energy lies the half-filled d_{xy} orbital. The insulator character of Sr_2IrO_4 comes from electron–electron correlation in the half-filled band. On the other hand, the rotation of the IrO_6 octahedra significantly changes the Ir–O–Ir bond angle, from 180° to approximately 158° (φ parameter in table 1), diminishing the electronic bandwidth due to decreased Ir–O–Ir orbital overlap, and contributing at the same time to the electron–electron correlation in Sr_2IrO_4. The incorporation of La atoms into the crystal structure produces Ir^{3+} with an array $t_{2g}^6e_g^0$, which in the IrO_2 layer should enhance the insulator character as x increases in $Sr_{2-x}La_xIrO_4$; figure 3 depicts this behaviour.

Even though the electronic structure of Sr_2IrO_4 is not yet available, experimental results suggest that the semiconducting behaviour of $Sr_{2-x}La_xIrO_4$ as a function of the La content, can be explained on the basis of a gapped system with localized states near the band edge, as suggested by Kini *et al* for Sr_2IrO_4 [28]. The effect of Sr substitution by La is to enhance such localized character at the IrO_2 layers.

3.4. Magnetic properties

Several zero field cooling (ZFC) and field cooling (FC) dc magnetic measurements were performed for a broad range of applied magnetic-field strengths. Figure 4 shows the temperature dependence of the magnetic susceptibility $\chi(T)$ of $Sr_{2-x}La_xIrO_4$. All measurements were made in a field of 10 kOe in both zero field cooling (ZFC) and field cooling (FC) routes. All data shown have been corrected for core diamagnetism, $(1.07 + 0.11x) \times 10^{-4}$ emu mol^{-1} [30]. For $x = 0$, Sr_2IrO_4, a clear magnetic transition around 240 K is observed. This same value has been reported for both polycrystalline [1, 10, 13, 29] and

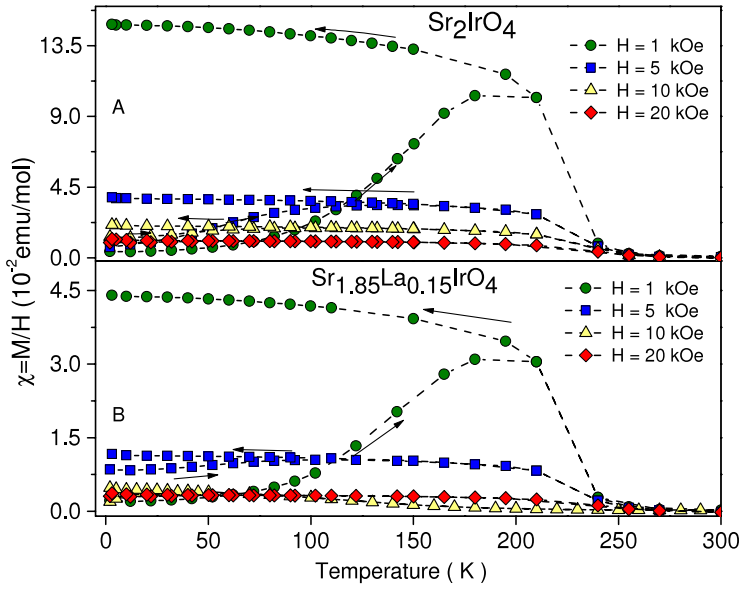

Figure 5. Temperature dependence of the magnetic susceptibility (A) for Sr_2IrO_4, (B) for $Sr_{1.85}La_{0.15}IrO_4$ under different magnetic fields. This plot shows how the IT diminishes with the applied magnetic field. These IT values were used to fit the Almeida–Thouless equation for Sr_2IrO_4.

single crystal samples [29]. Samples containing lanthanum, $x \neq 0$, show the same behaviour, but as the lanthanum content increases such transition becomes smoother and wider, and the inflection point in such curves moves toward lower temperatures. In order to understand the nature of the magnetic transition and the role played by the lanthanum atoms in the structure, compounds with $x = 0$ and 0.15 were analysed. First, measurements of the temperature dependence of magnetization in different external fields were performed (1, 5, 10, and 20 kOe, figure 5), followed by isothermal magnetization measurements for the same samples at several temperatures (figure 7).

Shown in figure 4 is the temperature dependence of magnetic susceptibility of $Sr_{2-x}La_xIrO_4$. Here, an irreversible behaviour, characteristic of weak ferromagnetism, can be observed. From the plot, the La-content effect on the irreversibility temperature (IT), i.e. the temperature at which the ZFC and FC magnetization data begin to deviate from one another, is also evident. As shown in figure 4, the observed values of magnetic susceptibility are of the order of those present in 3d TMO. To analyse the susceptibilities above the ferromagnetic transition, magnetic data were fitted to the Curie–Weiss behaviour, $\chi = \chi_0 + C/(T - \Theta)$, where χ_0 is the temperature independent susceptibility, C the Curie constant, and Θ the Curie–Weiss temperature. The effective paramagnetic moment in Sr_2IrO_4 is $\mu_{\text{eff}} \sim 0.5$ Bohr magnetons $(\mu_B)/Ir^{4+}$ which is too small as compared with the expected value of 1.73 μ_B for $S = 1/2$. This reduction of μ_{eff} has been suggested as indicative of a strong hybridization between 5d Ir and 2p oxygen orbitals [15]. On the other side, the value for the effective magnetic moment of Ir^{4+} in the $x = 0$ sample is the same as that reported for the measurement on the single crystal Sr_2IrO_4 [15]; those found for $Sr_{2-x}La_xIrO_4$ are 0.49, 0.46, and 0.44 μ_B/Ir for $x = 0.05$, 0.1, and 0.15, respectively. In the case of the solid solution $Sr_{2-x}La_xIrO_4$, the diminution of the μ_{eff} agrees with the increment of Ir^{3+} produced by La^{3+} introduced into the crystal cell. The values obtained for Θ were 209, 162, and 157 K for the corresponding x-values.

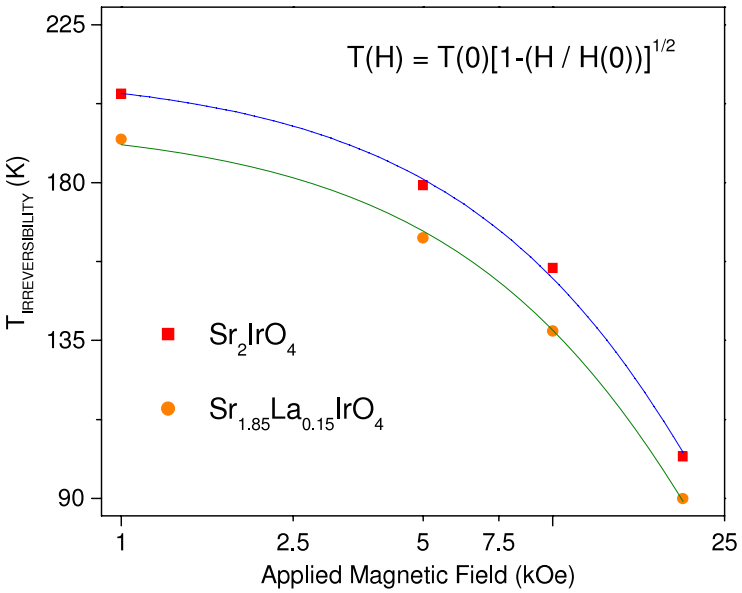

Figure 6. Irreversibility temperature (IT) versus applied magnetic field for Sr_2IrO_4 and $Sr_{1.85}La_{0.15}IrO_4$; the continuous line is a fit to the quasi-de Almeida–Thouless equation.

As shown in figure 4, both magnetic susceptibility and IT strongly depend on the La-composition. The IT dropping in $Sr_{2-x}La_xIrO_4$ (figure 4, $H = 10$ kOe) is probably related to the Ir^{3+} content, which in the low spin configuration is a diamagnetic ion. A plausible explanation can be obtained by following the ZFC curve, in which the sample exhibits a canted antiferromagnetic (AF) order. Here, the diamagnetic Ir^{3+} ions are not contributing to the magnetic coupling (Ir^{4+}); in this way the AF coupling is weakened and the Néel temperature drops, which can also be associated with the trend shown by the Θ values of $Sr_{2-x}La_xIrO_4$.

Figure 5 shows the magnetic susceptibility measurements for the solid solution $Sr_{2-x}La_xIrO_4$ ($x = 0$ and 0.15). As can be observed from these plots, in agreement with the Ir^{4+} content, the values for $x = 0$ are considerably higher (3–4 times) than for $x = 0.15$; for the IT the values are also higher. The dependence of IT on the applied magnetic field for the solid solution $Sr_{2-x}La_xIrO_4$ ($x = 0$ and 0.15) is illustrated in the magnetic susceptibility plots of figure 5. These graphs show that in both cases as the applied magnetic field increases, the IT moves toward lower temperatures and the differences between both paths, ZFC and FC, diminish. This trend can be easily understood by recognizing this as a typical characteristic of weak ferromagnetic behaviour. For sufficiently strong magnetic fields, the weak ferromagnetic component becomes totally saturated and there is no longer any path distinction between reversible and irreversible behaviour; the two curves will exactly coincide on top of each other [31].

Shown in figure 7(A) are the isothermal magnetization curves (M versus H) of Sr_2IrO_4 in fields of $0 \leqslant H \leqslant 40$ kOe. Here, the bulk ferromagnetic character of this sample is clear. The inset plot is the temperature dependence of the coercitive field (H_c) of samples, the extrapolated zero value of H_c is at $T = 70$ K. The isothermal magnetization for $x = 0.15$ in $Sr_{2-x}La_xIrO_4$ is shown in figure 7(B). As can be observed from this plot, the values for H_c are of the same order as those for $x = 0$, but, as expected for a lower saturation moment, the remanence (B_R) is lower. Although H_c and B_R are independent parameters that can be altered by heat treatments,

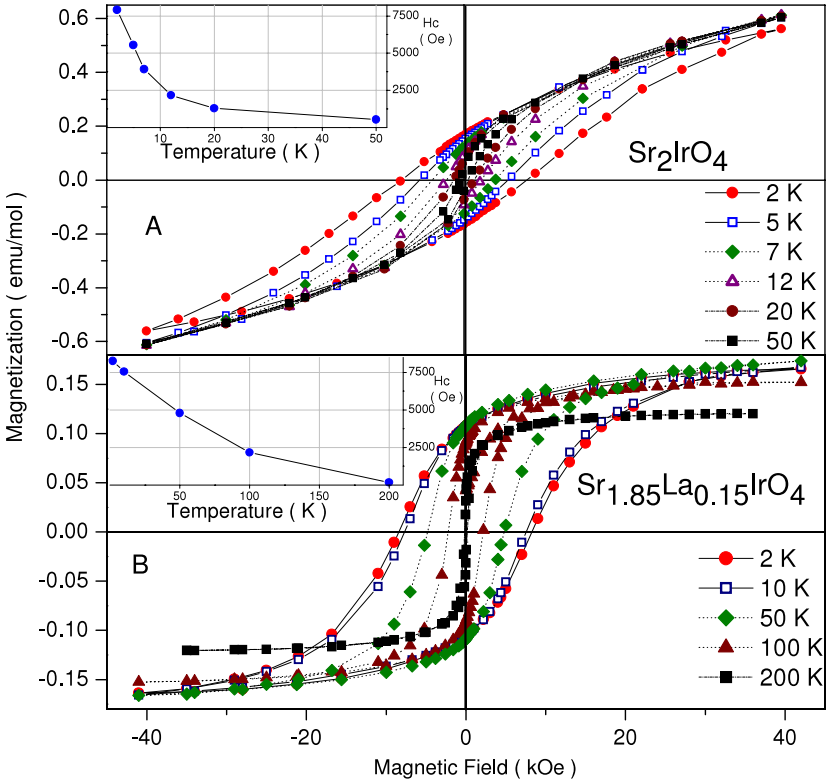

Figure 7. Magnetization isotherms (A) for Sr_2IrO_4 and (B) for $Sr_{1.85}La_{0.15}IrO_4$; the inset plot shows the coercitive field.

the observed trend can be considered congruent with the fact that the nonmagnetic ion Ir^{3+} is occupying the magnetic position of Ir^{4+} in the crystal cell. In both samples ($x = 0$ and 0.15), it is possible to observe that for a magnetic field up to $H = 40$ kOe saturation was not reached. By fitting the IT values to a quasi-de Almeida–Thouless relationship, see figure 6, [31, 32], the saturation magnetic field estimated is 66.2 kOe for $x = 0$, and 61.1 for $x = 0.15$; the regression coefficients were of the order of 0.998 for $n = 2$ in the quasi-de Almeida–Thouless equation. For Sr_2IrO_4, the estimated ferromagnetic moment $\mu_{\text{ferro}} = 0.023\ \mu_B/\text{Ir}$, is nearly negligible when compared to 1 μ_B expected for $S = 1/2$. In $Sr_{2-x}La_xIrO_4$, magnetic susceptibility plots indicate that the saturation moments are 0.18, 0.13, 0.05, 0.04, and 0.05 μ_B/Ir for $x = 0.0$, 0.05, 0.10, 0.15, and 0.20, respectively. The trend observed in these values is consistent with the assumption that the Ir^{4+}/Ir^{3+} ratio diminishes with La content in samples.

It is worth mentioning here the recent report of Nagai *et al* on the antiferromagnetic ground state of $Sr_3Ir_2O_7$ [33], since this system is the analogous $n = 2$ compound of the Ruddlesden–Popper series $Sr_{n+1}Ir_nO_{3n+1}$. There are several structural and electronic features shared between this compound and Sr_2IrO_4 ($n = 1$ case) [34]; both of them show weak ferromagnetism ($T_C \sim 280$ K for $Sr_3Ir_2O_7$) with only a small fraction of the expected ordered moment ($2 \times 10^{-3}\ \mu_B/\text{Ir}$ for $Sr_3Ir_2O_7$ below T_C). Also in $Sr_3Ir_2O_7$ the observed weak ferromagnetism is derived from canted antiferromagnetism (DM interaction) with no evidence of structural phase transition at T_C [33].

4. Conclusions

Compounds of the solid solution $Sr_{2-x}La_xIrO_4$ can be prepared in the range of $0 \leqslant x \leqslant 0.20$ in polycrystalline single-phase. After the electrochemical analyses that corroborate the presence of Ir^{4+}/Ir^{3+} in the $Sr_{2-x}La_xIrO_4$ system, it is clear that the structure, magnetic and electrical properties of such a system are strongly influenced by the La content of samples via the Ir^{4+}/Ir^{3+} ratio.

From the structural point of view, the La content in the solid solution $Sr_{2-x}La_xIrO_4$ diminishes the Ir^{4+} content in samples; in this way, there is a reduction of the unit cell *c*-axis due to the cancellation of the Jahn–Teller distortion of the IrO_6 octahedra. According to the structural refinements, there is a modest increment of the Ir–O–Ir bond angle, which produces an increase of the in-plane cell parameters; on the other hand, this change does not affect the weak ferromagnetic behaviour of the solid solution.

Electrical conductivity does not seem to correlate with the Ir–O–Ir bond angle, but it correlates with the Ir^{3+} content, since the electronic configuration for this cation, $t_{2g}^6e_g^0$, would imply the existence of a larger gap. Activation energy values are in the order of those observed for $Sr_{2-x}A_xIrO_4$ (A = Ca and Ba), but in $Sr_{2-x}La_xIrO_4$ these values increase with the La (Ir^{3+}) content.

Magnetic susceptibility and isothermal magnetization of $Sr_{2-x}La_xIrO_4$ ($x = 0$ and 0.15) reflect the bulk nature of a weak ferromagnetism below 240 K. The weak ferromagnetism observed in $Sr_{2-x}La_xIrO_4$ is probably driven by the small ferromagnetic component present in an antiferromagnetically ordered spin system due to canting of the Ir^{4+} ordered moments.

Acknowledgments

We thank Dr Ernesto Zeller for his valuable comments, also to Q Arturo Garcia for his technical support in CPE voltammetry. This work was done with support from DGAPA-UNAM under projects PAPIIT IN105207-3 and IN101107-3.

References

[1] Crawford M K, Subramanian M A, Harlow R L, Fernandez-Baca J A, Wang Z R and Johnston D C 1994 *Phys. Rev.* B **49** 9198
[2] Rao C N R, Ganguly P, Singh K K and Mohan Ram R A 1988 *J. Solid State Chem.* **72** 14
Singh K K, Ganguly P and Goodenough J B 1984 *J. Solid State Chem.* **52** 254
[3] Kato S, Ogasawara M, Sugai M and Nakata S 2004 *Catal. Surveys from Asia* **8** 27
[4] Cao G, Crow J E, Guertin R P, Henning P F, Homes C C, Strongin M, Basov D N and Lochner E 2000 *Solid State Commun.* **113** 657
[5] Whangbo M H and Koo H J 2001 *Solid State Commun.* **118** 491
[6] Cao G, Xin Y, Alexander C S, Crow E, Schlottmann P, Crawford M K, Harlow R L and Marshall W 2002 *Phys. Rev.* B **66** 214412
[7] Cao G, Lin X N, Chikara S, Durairaj V and Elhami E 2004 *Phys. Rev.* B **69** 174418
[8] Yonesawa S, Muraoka Y, Matsuchita Y and Hiroi Z 2004 *J. Phys.: Condens. Matter* **16** L9
Yonesawa S, Muraoka Y, Matsuchita Y and Hiroi Z 2004 *J. Phys. Soc. Japan* **73** 1651
[9] Randall J J, Katz L and Ward R 1957 *J. Am. Chem. Soc.* **79** 266
Randall J J and Ward R 1959 *J. Am. Chem. Soc.* **81** 2629
[10] Cava R J, Batlogg B, Kiyono K, Takagi H, Krajewski J J, Peck W F, Rupp L W Jr and Chen C H 1994 *Phys. Rev.* B **49** 11890
[11] Huang Q, Soubeyroux J L, Chmaissen O, Natali Sora I, Santoro A, Cava R J, Krajewski J J and Peck W F Jr 1994 *J. Solid State Chem.* **112** 355
[12] Demazeau G, Buffat B, Pouchard M and Hagenmuller P 1984 *J. Solid State Chem.* **54** 389
[13] Shimura T, Inaguma Y, Nakamura T, Itoh M and Mori Y 1995 *Phys. Rev.* B **52** 9143

[14] Johnston D C, Ami T, Borsa F, Crawford M K, Fernandez-Baca J A, Kim K H, Harlow R L, Mahajan A V, Miller L L, Subramanian M A, Torgeson D R and Wang Z R 1994 *Proc. 17th Int. Taniguchi Symp. on Theoretical Physics on 'Spectroscopy of Mott Insulators and Correlated Metals' (Shima, Oct. 1994)*
[15] Cao G, Bolivar J, McCall S, Crow J E and Guertin R P 1998 *Phys. Rev.* B **57** R11039
[16] Dzialoshinski I 1958 *J. Phys. Chem. Solids* **4** 241
[17] Moriya T 1960 *Phys. Rev.* **120** 91
[18] Katsura H, Nagaosa N and Balatsky A 2005 *Phys. Rev. Lett.* **95** 057205
[19] Ramírez M T, Palomar M E, González I and Rojas-Hernández A 1995 *Electroanalysis* **7** 184
[20] Kalcher K 1990 *Electroanalysis* **2** 419
[21] Shimura T, Inaguma Y, Nakamura T, Itoh M and Mori Y 1995 *Phys. Rev.* B **52** 9143
[22] Blaha P, Schwarz K, Madsen G K H, Kvasnicka D and Luitz J 2001 *WIEN2k, An Augmented Plane Wave + Local Orbitals Program for Calculating Crystal Properties* (Austria: Karlheinz Schwarz, Techn. Universität Wien) ISBN 3-9501031-1-2
[23] Perdew J P, Burke K and Ernzerhof K 1996 *Phys. Rev. Lett.* **77** 3865
[24] Young R A, Sakthivel A, Moss T S and Paiva-Santos C O 1995 *J. Appl. Crystallogr.* **28** 366
[25] Shannon R D 1976 *Acta Crystallogr.* A **32** 751
[26] Cosio-Castañeda C, Baeza A, de la Mora P and Tavizon G 2007 in preparation
[27] Cosio-Castañeda C 2006 *MSc Thesis* UNAM
[28] Kini N S, Stridom A M, Jeevan H S, Geibel C and Ramakrishnan S 2006 *J. Phys.: Condens. Matter* **18** 8205
[29] Cao G, Bolivar J, McCall S, Crow J E and Guertin R P 1998 *Phys. Rev.* B **57** R11039
[30] O'Connor C J 1982 Magnetochemistry—advances in theory and experimentation *Prog. Inorg. Chem.* **29** 203
[31] Bennahmias M, Radousky H B, Buford C M, Kebede A B, McIntyre M, Goodwin T J and Shelton R N 1996 *Phys. Rev.* B **53** 2773
[32] Morgenstern I, Muller K A and Bednorz J G 1988 *Physica* C **153–155** 59
[33] Nagai I, Yoshida Y, Ikeda S I, Matsuhata H, Kito H and Kosaka M 2007 *J. Phys.: Condens. Matter* **19** 1
[34] Cao G, Xin Y, Alexander C S, Crow J E and Schlottmann P 2002 *Phys. Rev.* B **66** 214412